Spectroscopy of Nanoparticles without Light

Johannes Fiedler,[1,2,*] Clas Persson,[1] and Stefan Yoshi Buhmann[2,3]

[1] *Centre for Materials Science and Nanotechnology, Department of Physics, University of Oslo, P.O. Box 1048 Blindern, 0316 Oslo, Norway*

[2] *Physikalisches Institut, Albert-Ludwigs-Universität Freiburg, Hermann-Herder-Straße 3, 79104 Freiburg, Germany*

[3] *Freiburg Institute for Advanced Studies, Albert-Ludwigs-Universität Freiburg, Albertstraße 19, 79104 Freiburg, Germany*

(Received 26 September 2019; published 15 January 2020)

One of the most-important tools in modern science is the analysis of electromagnetic properties by spectroscopy. The various types of spectroscopy can be classified by the underlying type of interactions between energy and the material. In this paper we demonstrate a class of spectroscopy based on Casimir interactions between a solid investigated object and a reference surface embedded in an environmental liquid medium. Our main example is based on the measurement of Hamaker constants on change of the concentration of an intervening two-component liquid, where we demonstrate a possible reconstruction algorithm to estimate the frequency-dependent dielectric function of the particle investigated.

DOI: 10.1103/PhysRevApplied.13.014025

I. INTRODUCTION

Spectroscopy in general is a method to investigate a material's properties, in particular the electromagnetic properties for the characterization of an unknown material with respect to its constituents [1] (type and stoichiometry) and its optical behavior [2] (such as band gaps in semiconductors). A huge challenge is the experimental determination of the dielectric function $\varepsilon(\omega)$ of a material, which is due to, on the one hand, the large range of the electromagnetic spectrum and, on the other hand, the function being complex valued. In principle, the measurement of the dielectric function ensues by excitation of the system at the frequency investigated and measurement of its response. The complexity of such experiments is because each spectral range requires a different source for the exciting beam. For instance, measurements in the low-frequency range (radio waves), where the electromagnetic wave couples to the states of the core spin, require nuclear-magnetic-resonance spectroscopy [3–5], and measurements in the microwave region, where the electromagnetic wave couples to the electronic spin states and rotational states, require electron-paramagnetic-resonance spectroscopy [6]. The next spectral range is investigated by terahertz spectroscopy [7,8]. The infrared spectrum is investigated by infrared spectroscopy [9] and Raman spectroscopy [10], for instance. In the visible and ultraviolet ranges, ultraviolet-visible spectroscopy [11] or reflection spectroscopy [12] is typically used. Finally, x-ray spectroscopy and gamma spectroscopy [13] complete the investigation of the spectrum. To conclude, a huge number of different experiments have to be performed to measure the complete dielectric function of a material. The dielectric function, being complex, poses an additional challenge. For instance, by reflection spectroscopy one usually obtains the real part of the refractive index n and/or the attenuation coefficient k, which is connected to the absorption coefficient. The combination of both results is required to infer the dielectric function. However, often both ingredients are not simultaneously available, and one needs to apply the Kramers–Kronig relation [14,15], which requires knowledge of the complete spectrum for the imaginary or real part to calculate the respective other part.

However, alternatives exist in the form of experiments with high accuracy whose results directly depend on dynamical dielectric functions; for instance, Casimir-force experiments by atomic force microscopy in a vacuum [16,17] and in a medium [18]. Figure 1 illustrates the typical experimental setup. A spherical nanoparticle is attached to the cantilever of an atomic force microscope. The radius of the sphere should be large enough that effects caused by the curvature of the surface can be ignored. By changing the distance d between the sphere and the substrate, one can measure the Casimir force. In such experiments, one typically uses a sphere of large curvature radius to overcome the issue of arranging two parallel plates and applies the Lifshitz formula for the theoretical description.

*johannes.fiedler@physik.uni-freiburg.de

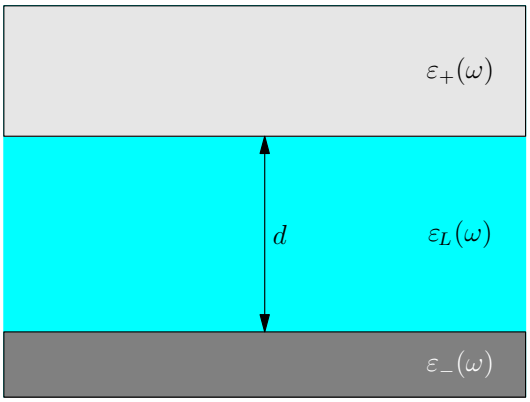

FIG. 1. Casimir-force experiments by atomic force microscopy. A sphere with dielectric function ε_+ and a large curvature radius is attached to a cantilever, which is closely separated from a substrate with dielectric function ε_-. By varying the distance between both objects, one can measure the Casimir force between them. Additional to the vacuum experiments, a liquid with dielectric function ε_L surrounds the particle.

In this paper we consider the above-mentioned Casimir-force experiment and show a possible way to extract the dielectric function of one plate from the measured Casimir-force data. To vary the Casimir force, we assume a liquid consisting of two components is surrounding the sphere; hence, the observed force depends on the concentration of the two liquids. We consider a simple example to illustrate the method with a textbook inversion procedure to infer the dielectric constant from the force data. The method can easily be extended beyond this proof-of-principle demonstration to increase the precision or for generalization to other measurement setups.

II. THEORY AND RECONSTRUCTION METHOD

A. Casimir effect in media

The Casimir effect, the typically attractive force between two dielectric plates with permittivities ε_- (bottom plate) and ε_+ (top plate) separated by a distance d with a medium permittivity ε_L, can be described by the sum over the exchange of virtual photons between them [19–21]:

$$f(d) = -\frac{k_B T}{\pi}{\sum_{m=0}^{\infty}}' \int_0^{\infty} dk^{\parallel} k^{\parallel} \kappa^{\perp} \sum_{\sigma=s,p} \frac{r_\sigma^+ r_\sigma^- e^{-2\kappa^{\perp} d}}{D_\sigma}, \quad (1)$$

where k_B is the Boltzmann constant, T is the temperature, the primed sum denotes that the first term has to be weighted by 1/2, $\xi_m = 2\pi k_B T m/\hbar$ are the Matsubara frequencies, $D_\sigma = 1 - r_\sigma^+ r_\sigma^- e^{-2\kappa^{\perp} d}$ are the multiple reflection terms, and $\kappa_i^{\perp} = \sqrt{k^{\parallel 2} + \varepsilon_i \xi^2/c^2}$ is the imaginary part of the transverse wave vector. The coefficients r_σ^+ and r_σ^- are the generalized reflection coefficients at the interfaces for p- and s-polarized waves [22,23]

$$r_p^i = \frac{\varepsilon_L \kappa_i^{\perp} - \varepsilon_i \kappa_L^{\perp}}{\varepsilon_L \kappa_i^{\perp} + \varepsilon_i \kappa_L^{\perp}}, \qquad r_s^i = \frac{\kappa_i^{\perp} - \kappa_L^{\perp}}{\kappa_i^{\perp} + \kappa_L^{\perp}}, \quad (2)$$

respectively. In the nonretarded limit, the z component of the Casimir-force density reads

$$f(d) = -\frac{H}{6\pi d^3}, \quad (3)$$

with the Hamaker constant

$$H = \frac{3k_B T}{2}{\sum_{m=0}^{\infty}}' \frac{\mathrm{Li}_3[r_p^+(i\xi_m) r_p^-(i\xi_m)]}{\varepsilon_L(i\xi_m)}, \quad (4)$$

where the polylogarithmic function

$$\mathrm{Li}_3(y) = 4\int_0^{\infty} dx x^2 \frac{y e^{-2x}}{1 - y e^{-2x}} \quad (5)$$

and the nonretarded reflection coefficients for p-polarized waves

$$r_p^{\pm} = \frac{\varepsilon_{\pm} - \varepsilon_L}{\varepsilon_{\pm} + \varepsilon_L}. \quad (6)$$

The estimation of the Hamaker constant by experiments of this type is very accurate, which decreases the errors of the reconstruction method as one can assume that the measured Hamaker constants are precisely measured. Current experiments report deviations below 5% depending on the surface roughness, spatial resolution, and error of the spring constant [24].

B. Mixing of fluids

To introduce a tunable parameter, we consider a two-component fluid between both plates. For the dielectric functions of mixtures of fluid 1 (ε_1) in fluid 2 (ε_2) we use a Lorentz-Lorenz-like model [25]:

$$\varepsilon_L = \frac{1 + 2\tilde{\alpha}}{1 - \tilde{\alpha}}, \quad \tilde{\alpha} = p\frac{\varepsilon_1 - 1}{\varepsilon_1 + 2} + (1 - p)\frac{\varepsilon_2 - 1}{\varepsilon_2 + 2}, \quad (7)$$

where p is the volume fraction of fluid 1 in fluid 2. To illustrate the results, we choose the liquids bromobenzene and methanol in front of a polystyrene surface [18]. Figure 2 illustrates the resulting dielectric function. One observes a change of the crossings of the dielectric functions depending on the volume fraction by following the intersection of the colored surface (liquid) and the gray slightly transparent surface (polystyrene).

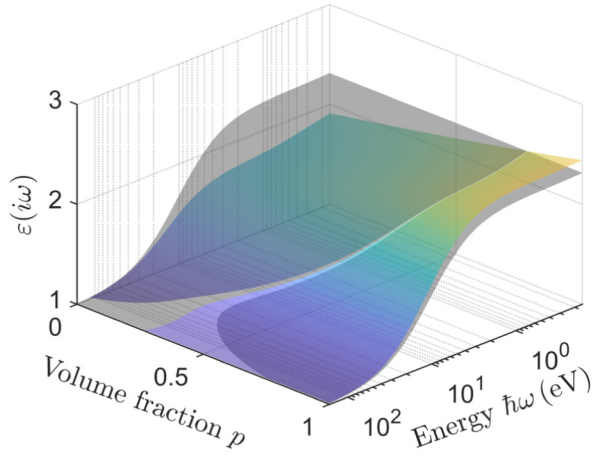

FIG. 2. Dependence of the effective dielectric function $\varepsilon_L(i\xi,p)$ of the mixed components methanol and bromobenzene on the volume fraction p. To illustrate the crossings in the dielectric function, the gray surface denotes the permittivity of polystyrene $\varepsilon_-(i\xi)$.

C. Repeated measurements with changed concentration

The result of repeated measurements with different concentrations is a series of Hamaker constants

$$H(p) = \frac{3k_BT}{2} \times \sum_{m=0}^{\infty}{}' \frac{1}{\varepsilon_L(p)} \mathrm{Li}_3\left[\frac{\varepsilon_+ - \varepsilon_L(p)}{\varepsilon_+ + \varepsilon_L(p)} \frac{\varepsilon_- - \varepsilon_L(p)}{\varepsilon_- + \varepsilon_L(p)}\right], \quad (8)$$

with ε_+ being the target dielectric function. In general, this function maps uniquely the target dielectric function onto the set of Hamaker constants, because reflection coefficients are typically bounded by $|r| \leq 1$, which allows the Taylor-series expansion of the polylogarithmic function.

To illustrate the reconstruction method, we calculate the Hamaker constants for different volume fractions with a plate, where the target dielectric function to be reconstructed is given by a damped two-oscillator model:

$$\varepsilon_+(i\omega) = 1 + \sum_j \frac{c_j}{1 + \gamma_j\omega + (\omega/\omega_j)^2} \quad (9)$$

with $c_1 = 2$, $c_2 = 1.5$, $\omega_1 = 2$ eV, $\omega_2 = 6$ eV, $1/\gamma_1 = 50$ eV, and $1/\gamma_2 = 200$ eV, which are typical values for a dielectric body.

D. Reconstruction method

The inverse problem is now defined as calculating the dielectric function of the plate $\varepsilon_+(\omega)$ given knowledge of the Hamaker constants $H(p)$, the substrate dielectric function $\varepsilon_-(\omega)$, and the liquid dielectric function $\varepsilon_L(p,\omega)$ via Eq. (8). The dielectric function is a linear-response function and has to satisfy specific properties, which will be exploited by the reconstruction method. First, the dielectric function has to satisfy causality, which leads to the connection of its real and imaginary parts via the Kramers–Kronig relation,

$$\mathrm{Re}\,\varepsilon(\omega) = 1 + \frac{2}{\pi}\mathcal{P}\int_0^\infty \frac{\omega'\,\mathrm{Im}\,\varepsilon(\omega')}{\omega'^2 - \omega^2} d\omega', \quad (10)$$

$$\mathrm{Im}\,\varepsilon(\omega) = -\frac{2}{\pi}\mathcal{P}\int_0^\infty \frac{\omega'\,\mathrm{Re}\,\varepsilon(\omega')}{\omega'^2 - \omega^2} d\omega', \quad (11)$$

with the Cauchy principal value. By substituting $\omega = i\xi$ into Eq. (10), one can find the relation to imaginary arguments:

$$\varepsilon(i\xi) = 1 + \frac{2}{\pi}\int_0^\infty \frac{\omega'\,\mathrm{Im}\,\varepsilon(\omega')}{\omega'^2 + \xi^2} d\omega'. \quad (12)$$

Furthermore, the function is has to go to 1 for large frequency arguments, $\lim_{\omega\mapsto\infty}\varepsilon(\omega) = 1$. Another important property is the analyticity in the upper complex half-plane. This fact together with the causality leads to monotonic behavior on the imaginary-frequency axis. Because the dielectric function is a linear-response function, sum rules exist that also have to be satisfied [26].

The Hamaker constant $H(p)$, which is depicted in Fig. 3 for the material combination with a polystyrene substrate and a liquid mixture of bromobenzene and methanol (both depicted in Fig. 2) and the sphere with dielectric function (9), depends nonlinearly on the target function ε_+. Thus, we apply the Newton-Raphson method to Eq. (8), which transforms the nonlinearity into an iterative algorithm of systems of equations, which needs to be solved in the following way:

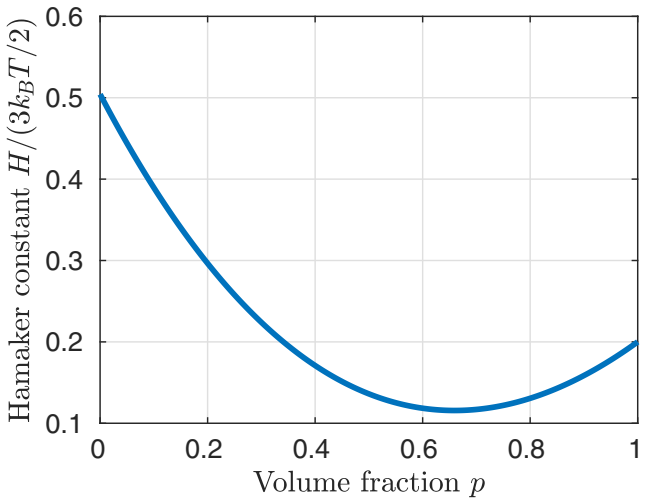

FIG. 3. Example of Hamaker constants between two dielectric plates embedded in a two-component liquid with the volume fraction p giving the ratio of bromobenzene in methanol.

(a) Initialization, where we choose

$$x_{0,i} = \varepsilon_+^{(0)}(i\omega_i) = 1 + \frac{A}{1 + (\omega_i/B)^2} \tag{13}$$

along a frequency grid of the first 200 Matzubara frequencies, with the parameters $A = 8$ and $B = 0.5$ eV.

This initial function is chosen to ensure the monotonic decrease of the dielectric function. The stability of the method strongly depends on the value of B. For large values, the function overestimates the high-frequency regime too much, leading to convergence to a false (local) minimum. For small values, this region is strongly depressed, stabilizing the method. In contrast, the amplitude chosen does not effect the stability of the method. Furthermore, the static dielectric constant is overestimated by $\varepsilon_+^{(0)}(0) = 9$. The target function to be determined has only $\varepsilon_+(0) = 4.5$. Simulations show that overestimation of the static value is easier to handle for the algorithm. To perform the method with an ordinary computer, we restrict ourselves to considering only the first 200 Matsubara frequencies (at room temperature), which covers the spectral range reaching the extreme ultraviolet, which covers most of the physical effects. This algorithm is followed by:

(b) Calculation of the matrix elements $D_{ij} = \partial H(p_i)/\partial\varepsilon_+(i\omega_j)$ to solve the system of equations

$$\mathbf{D}\Delta\mathbf{x}^{(i+1)} = H(p) - H(p, \Delta\mathbf{x}^{(i)}), \tag{14}$$

with the measured Hamaker constants $H(p)$ and the calculated Hamaker constants based on the previously iterated data according to Eq. (8).

The matrix **D** typically has singularities. To overcome this issue, we apply the Moore–Penrose pseudoinverse. It is known that Newton's method converges locally, which means that it strongly depends on the initial data. This effect is directly observable as oscillations in the target function, which violates the causality properties of the dielectric function mentioned above. To solve this issue, we regularly force the newly iterated function onto a causal monotonic profile by:

(c) Fitting the result to a strictly monotonically decreasing function:

$$x_j^{(i+1)} = x_j^{(i)} + \Delta x_j^{(i)} \approx 1 + \frac{\lambda_1}{1 + (\omega_j/\lambda_2)^2}, \tag{15}$$

with parameters λ_1 and λ_2.

We find that a fitting to this single-oscillator model, which satisfies the monotonic behavior, works optimally and reproduces the more-complicated two-oscillator target after the next iteration. This favorable behavior is caused by the large differences between the oscillator strengths in the example [Eq. (9)]. On smaller scales with two or more narrow peaks, we introduce a termination condition for the filter (c) according to the iteration step by:

(d) calculating the maximum iterative step size

$$\max_j \left|\Delta\varepsilon_+(i\omega_j)\right| < C, \tag{16}$$

which we chose in our case to be 0.1. By use of step sizes below this threshold, the fitting step (c) will be left out.

We also test the reconstruction method for models with more oscillators, and the data are reproduced with fewer than 100 iterations. The result of this reconstruction method with the target function (9) is depicted in Fig. 4. It can be observed that the target function is reproduced with six iterations. Especially, the regions around the two oscillators (at 2 and 6 eV) are well reproduced. A small deviation of the static value is observed. Even when the strength of the damping parameters in the model (9) is increased to absurdly high numbers, the reconstruction method yields a standard deviation below 1% between the reconstructed dielectric function and the target dielectric function. The most strongly affected data points are located in the infrared region, where the absolute deviation is still bounded by 10%. The inversion method presented has some limitations because of the possible reconstruction of completely unknown dielectric functions. In the way presented, the target dielectric function has to be quite smooth for it to be approximated by a single oscillator response function with respect to the condition given by Eq. (16). To take errors due to this condition into account, one needs

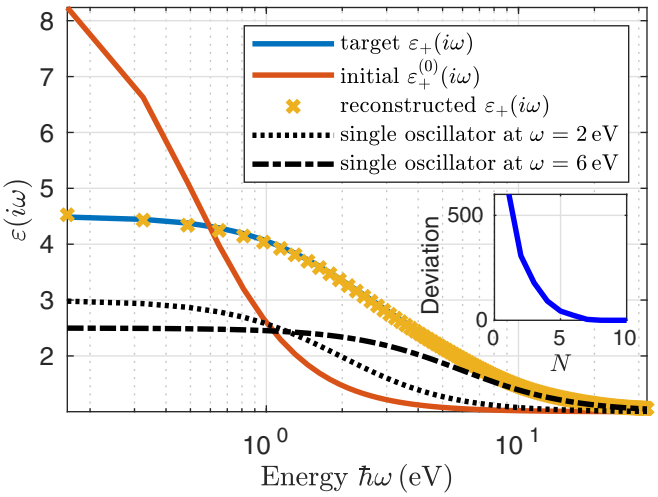

FIG. 4. Agreement of the reconstruction method: the target dielectric function (solid blue line) is well reproduced by the reconstructed dielectric function (yellow crosses). The initial dielectric function (solid red line) illustrates the convergence of the method. In the inset, the convergence of the method is depicted via the least squares of the target function and the reconstructed function in each iteration step.

the redo the calculation with different values. For generalization of this method to arbitrary response functions, one needs to record the oscillating profiles in between, where one observes fixed points that already match the target function. Thus, improvement of the method can be achieved with respect to two possibilities: (i) by optimizing the fitting in step (c) or (ii) by reducing the system of equations, step (b), to reproduce these values directly.

After the reconstruction of the target dielectric function on the imaginary-frequency axis $\varepsilon_+(i\xi)$, the result needs to be transformed to the real-frequency axis. This can be done via the integral equation (10) which is an inhomogeneous Fredholm equation of the first kind. This procedure results in the imaginary part of the dielectric function, and after the additional application of the Kramers–Kronig relation (10), its real part can be obtained.

III. CONCLUSIONS

We introduce a reconstruction method to estimate the dielectric function of a solid plate by established Casimir-force experiments. To estimate the dielectric function for 200 Matsubara frequencies, 200 Hamaker constants at different concentrations are required. For larger distances, the frequency and spatial dependences of the interaction do not separate [27], which can be exploited to reduce the number of experimental repetitions. A more-efficient reduction of the number of experiments toward an application of this method can be achieved by the training of a neuronal network, which will be investigated in further studies. Besides the introduced application of the reconstruction of the dielectric function of the attached nanoparticle, the method can directly be used to measure the dielectric function of the substrate and after some modification to measure the dielectric function of the liquid. The decomposition of the liquid or gas components will also be part of future investigations. Furthermore, this method can be adapted to low spectral ranges, terahertz radiation and below, where current methods fail, by combining the proposed method with experimentally obtained data from higher-energy ranges. If the system is cooled down to several kelvins, the natural discretization yields roughly 100 points covering the terahertz regime. Further cooling will lead to a transition to the 0-K Casimir force, where the discrete sum has to be exchanged by the continuous integral, which results in a free parameterization for the regime investigated depending on knowledge of further optical data. Experimentally challenging is the control of two liquids at the required low temperatures, which can be done by use of superfluids or ultracold quantum gases.

ACKNOWLEDGMENTS

We acknowledge support from the Research Council of Norway (project No. 250346). We gratefully acknowledge support by the German Research Council (Grant No. BU 1803/6-1 to S.Y.B. and J.F. and Grant No. BU 1803/3-1 to S.Y.B.).

[1] B. Welz and M. Sperling, *Atomic Absorption Spectrometry* (WILEY–VCH, Weinheim, 1998).
[2] C. S. Granerød, B. L. Aarseth, P. D. Nguyen, C. Bazioti, A. Azarov, B. G. Svensson, L. Vines, and Ø. Prytz, Structural and optical properties of individual Zn_2GeO_4 particles embedded in ZnO, Nanotechnology **30**, 225702 (2019).
[3] F. Bloch and A. Siegert, Magnetic resonance for nonrotating fields, Phys. Rev. **57**, 522 (1940).
[4] L. W. Alvarez and F. Bloch, A quantitative determination of the neutron moment in absolute nuclear magnetons, Phys. Rev. **57**, 111 (1940).
[5] E. M. Purcell, H. C. Torrey, and R. V. Pound, Resonance absorption by nuclear magnetic moments in a solid, Phys. Rev. **69**, 37 (1946).
[6] E. Zavoisky, Paramagnetic absorption in some salts in perpendicular magnetic fields, Zhur. Eksperiment. i Theoret. Fiz. **16**, 603 (1946).
[7] F. Junginger, A. Sell, O. Schubert, B. Mayer, D. Brida, M. Marangoni, G. Cerullo, A. Leitenstorfer, and R. Huber, Single-cycle multiterahertz transients with peak fields above 10 MV/cm, Opt. Lett. **35**, 2645 (2010).
[8] R. Buchner, J. Barthel, and J. Stauber, The dielectric relaxation of water between 0 °C and 35 °C, Chem. Phys. Lett. **306**, 57 (1999).
[9] C. Christiansen, Untersuchungen über die optischen Eigenschaften von fein vertheilten Körpern, Ann. Phys. **260**, 439 (1885).
[10] I. D. Wolf, Micro-Raman spectroscopy to study local mechanical stress in silicon integrated circuits, Semicond. Sci. Technol. **11**, 139 (1996).
[11] H. Stranneheim and J. Lundeberg, Stepping stones in DNA sequencing, Biotechnol. J. **7**, 1063 (2012).
[12] J. L. Koenig, in *Spectroscopy of Polymers*, edited by J. L. Koenig (Elsevier Science, New York, 1999), 2nd ed., pp. 77–145.
[13] G. R. Gilmore, *Practical Gamma-Ray Spectrometry* (John Wiley & Sons, Chichester, 2008).
[14] R. de L. Kronig, On the theory of dispersion of x-rays, J. Opt. Soc. Am. **12**, 547 (1926).
[15] H. Kramers, La diffusion de la lumière par les atomes, Atti Cong. Intern. Fisici **2**, 545 (1927).
[16] P. S. Davids, F. Intravaia, F. S. S. Rosa, and D. A. R. Dalvit, Modal approach to Casimir forces in periodic structures, Phys. Rev. A **82**, 062111 (2010).
[17] P. Loskill, C. Zeitz, S. Grandthyll, N. Thewes, F. Müller, M. Bischoff, M. Herrmann, and K. Jacobs, Reduced adhesion of oral bacteria on hydroxyapatite by fluoride treatment, Langmuir **29**, 5528 (2013).
[18] P. J. van Zwol and G. Palasantzas, Repulsive Casimir forces between solid materials with high-refractive-index intervening liquids, Phys. Rev. A **81**, 062502 (2010).
[19] I. Brevik and S. A. Ellingsen, Comment on "Casimir force acting on magnetodielectric bodies embedded in media", Phys. Rev. A **79**, 027801 (2009).

[20] S. Y. Buhmann, *Dispersion Forces I: Macroscopic Quantum Electrodynamics and Ground-state Casimir, Casimir–Polder and van der Waals Forces* (Springer, Heidelberg, 2012).

[21] F. A. Burger, J. Fiedler, and S. Y. Buhmann, Zero-point electromagnetic stress tensor for studying Casimir forces on colloidal particles in media, Europhys. Lett. **121**, 24004 (2018).

[22] M. S. Tomaš, Green function for multilayers: Light scattering in planar cavities, Phys. Rev. A **51**, 2545 (1995).

[23] W. Chew, *Waves and Fields in Inhomogeneous Media* (Institute of Electrical & Electronics Engineers (IEEE), New York, 1995).

[24] M. Sedighi, V. B. Svetovoy, and G. Palasantzas, Casimir force measurements from silicon carbide surfaces, Phys. Rev. B **93**, 085434 (2016).

[25] D. E. Aspnes, Local-field effects and effective-medium theory: A microscopic perspective, Am. J. Phys. **50**, 704 (1982).

[26] C. Ambrosch-Draxl and J. O. Sofo, Linear optical properties of solids within the full-potential linearized augmented planewave method, Comput. Phys. Commun. **175**, 1 (2006).

[27] J. Fiedler, W. Broer, and S. Scheel, Reconstruction of Casimir—Polder interactions from matter-wave interference experiments, J. Phys. B Atom. Mol. Opt. Phys. **50**, 155501 (2017).